Attosecond and zeptosecond x-ray pulses via nonlinear Thomson backscattering

Pengfei Lan, Peixiang Lu,* Wei Cao, and Xinlin Wang
State Key Laboratory of Laser Technology and Wuhan National Laboratory for Optoelectronics, Huazhong University of Science and Technology, Wuhan 430074, People's Republic of China

(Received 11 April 2005; revised manuscript received 26 September 2005; published 14 December 2005)

Nonlinear Thomson backscattering of an intense circularly polarized laser by a counterpropagating energetic electron is investigated. The results show that in the scattering of a non-tightly-focused laser pulse with an intensity around 10^{19} W/cm^2 and a pulse duration of 100 fs full width at half maximum by a counterpropagating electron with an initial energy of 10 MeV, a crescent-shaped pulse with a pulse duration of 469 as and the photon energy ranging from 230 eV to 2.5 keV is generated in the backward direction. It is shown that the radiated pulse shape and monochromaticity can be modified by changing the laser beam waist, while in the case of a tightly focused laser field, a single peak pulse with a shorter duration and better monochromaticity can be obtained. With increase of the electron initial energy, the peak power of the radiated pulse increases and the pulse duration decreases. An isolated powerful zeptosecond (10^{-21} s) pulse with a peak power of about 10^{10} W/rad^2 and photon energy up to several MeV can be obtained with a 250 MeV electron.

DOI: 10.1103/PhysRevE.72.066501 PACS number(s): 41.60.−m, 42.65.Re, 52.59.Px

I. INTRODUCTION

The development of ultrashort intense laser technology has opened a new branch of research, attosecond physics. In this regime, ultrashort electromagnetic pulses, especially an isolated attosecond (as) pulse, have always been of keen interest, largely as a potential means of investigating and controlling ultrafast processes on the molecular and electron levels [1–3]. Up to now, various schemes have been explored for the generation of attosecond pulses. Farkas *et al.* [4] proposed a scheme based on laser induced high order harmonics, which is currently under intense investigation [5–8]. Other schemes for attosecond pulse generation include Fourier synthesis [9], stimulated Raman scattering [10], molecular modulation [11,12], and Thomson scattering [13]. In a breakthrough work [14], a train of 250 as pulses has been observed experimentally. However, all these methods have in theory a tendency to produce a train of closely spaced pulses rather than a single pulse. Potential methods to obtain a single attosecond pulse are mainly based on high order harmonics. Corkum *et al.* [16] suggested the usage of laser fields with a time-modulated degree of ellipticity to generate a single pulse from the attosecond pulse train. A more direct method for single attosecond pulse generation is based on the high order harmonics generated in ultrashort laser-atom interactions [17,18]. Another scheme is using the supercritical plasma [19]. With particle-in-cell simulations, Naumova *et al.* [19] found that a single 200 as pulse could be produced efficiently in a λ^3 laser pulse reflection, via deflection and compression from the relativistic plasma mirror created by the pulse itself. So far the only experimental indication for the single attosecond pulse was demonstrated by Hentschel *et al.* [15]; they observed a 650 as pulse at 90 eV photon energy driven by a 7 fs laser pulse. Moreover, the further time scale of fundamental interest is that of strong nuclear interactions which is in the 10^{-21} s [zeptosecond (zs)] domain. This temporal structure was first proposed by Kaplan *et al.* [20]. They pointed out that by focusing a perawatt or multiterawatt laser beam on a subwavelength-size solid particle or thin wire, electromagnetic bursts with time scale of 10^{-21}–10^{-22} s can theoretically be obtained.

The spectral character of nonlinear Thomson scattering was studied by many authors for its possible application as an x-ray source [21–28]. Hartemann [25] proposed a way to generate a narrow x-ray pulse by shaping the temporal envelope of the driving laser pulse. However, the corresponding temporal character has not attracted much attention. Recently Lee *et al.* [13] investigated the temporal characteristics of the radiation generated from relativistic nonlinear Thomson scattering by a stationary electron in a planar electromagnetic wave. A train of attosecond pulses with photon energy from 100 to 600 eV was obtained. By taking into account the effect of multielectrons, they proposed a method to enhance the radiation power [29]. In this paper, we investigate the Thomson backscattering of an intense circularly polarized laser by a counterpropagating energetic electron. The results show that a single attosecond pulse can be obtained in the scattering of a laser pulse with an intensity of 10^{19} W/cm^2 and a pulse duration of 100 fs by an electron with an initial energy of 10 MeV. A single powerful zeptosecond pulse is obtained when the initial electron energy increases to 250 MeV. Moreover, the spectra of these emitted ultrashort pulses as well as the behavior of the spectral phases of the radiations are discussed. It is shown that the radiated pulse shape and monochromaticity can be modified by changing the laser beam waist. Finally the dependence of the radiated power on various parameters is discussed as well.

II. FORMULATION

For a circularly polarized Gaussian laser pulse, the transverse components of the vector potential can be expressed as [30,31]

*Author to whom correspondence should be addressed. Email address: lupeixiang@hust.edu.cn

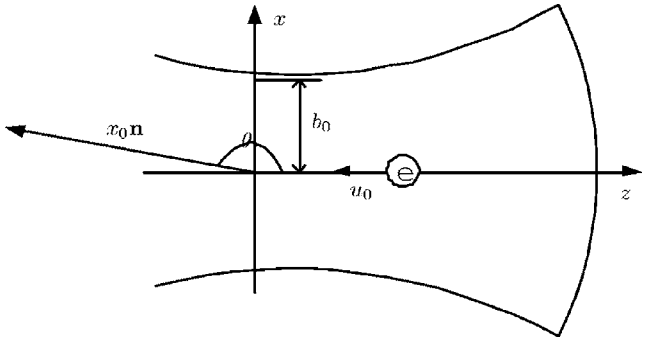

FIG. 1. Schematic geometry for Thomson scattering. The circularly polarized laser put at (0,0,0) propagates along the $+\hat{\mathbf{z}}$ direction. The electron moves in the $-\hat{\mathbf{z}}$ direction with an initial energy of γ_0. The electron is put at $(0,0,z_0)$ initially where $z_0=10L$.

$$\mathbf{a}_\perp = a_L\hat{\mathbf{a}}, \tag{1}$$

$$a_L = a_0 \exp(-\eta^2/L^2 - \rho^2/b^2)(b_0/b), \tag{2}$$

where $\hat{\mathbf{a}}=[\cos(\phi)\hat{\mathbf{x}}+\sin(\phi)\hat{\mathbf{y}}]$, $\rho^2=x^2+y^2$, $\exp(-\eta^2/L^2)$ is the Gaussian pulse shape function, the pulse duration is about $2L$, b is the radius of the spot size at position z, a_0 is the laser peak amplitude normalized by mc^2/e, $b=b_0(1+z^2/z_f^2)^{1/2}$, b_0 is the beam waist, and $z_f=b_0^2/2$ is the corresponding Rayleigh length. $\phi=\phi_p-\phi_G-\phi_0+\phi_R$, where $\phi_P=z-t=\eta$, $\phi_G=\tan^{-1}z/z_f$, $\phi_R=(x^2+y^2)/[2R(z)]$, and $R(z)=z(1+z_f^2/z^2)$. In the above definitions, space and time coordinates are normalized by k_0^{-1} and ω_0^{-1}, respectively, and ω_0 and k_0 are the laser frequency and wave number, respectively. m and $-e$ are the electron's mass and charge, respectively. The longitudinal component of the vector potential is expressed as [30,31]

$$a_z = a_L\left(-\frac{2x}{b_0 b}\sin(\phi+\theta)+\frac{2y}{b_0 b}\cos(\phi+\theta)\right), \tag{3}$$

where $\theta=\pi-\tan^{-1} z/z_f$.

The motion of an electron in an intense laser field is described by the following relativistic equations [32]:

$$\dot{\mathbf{p}}-\dot{\mathbf{a}} = -\nabla_a(\mathbf{u}\cdot\mathbf{a}), \tag{4}$$

$$\dot{\gamma} = \mathbf{u}\cdot\partial_t\mathbf{a}, \tag{5}$$

where $\mathbf{a}$ is the vector potential expressed by Eqs. (1)–(3), $\mathbf{u}$ is the velocity of the electron normalized by c, $\mathbf{p}=\gamma\mathbf{u}$ is the momentum normalized by mc, $\gamma=(1-u^2)^{-1/2}$ is the relativistic factor, and ∇_a in Eq. (4) acts on $\mathbf{a}$ only.

The angular distribution of the radiated power detected far away from the electron toward the direction $\mathbf{n}$ (see Fig. 1) at the time t can be calculated as [33]

$$\frac{dP(t)}{d\Omega} = |\mathbf{A}(t)|^2, \tag{6}$$

$$\mathbf{A}(t) = \left(\frac{\mathbf{n}\times\{[\mathbf{n}-\mathbf{u}(t')]\times\dot{\mathbf{u}}(t')\}}{[1-\mathbf{u}(t')\cdot\mathbf{n}]^3}\right)_{ret}, \tag{7}$$

where $dP(t)/d\Omega$ is normalized by $e^2\omega_0^2/4\pi c$, the subscript *ret* means that the quantities on the right hand should be evaluated at the retarded time t', t' is related to t by $t=t'+x_0-\mathbf{n}\cdot\mathbf{r}$, x_0 is the distance from the detector to the origin, $\mathbf{r}$ is the electron's displacement, and the radiation is detected in the direction $\mathbf{n}=\sin\theta\hat{\mathbf{x}}+\cos\theta\hat{\mathbf{z}}$ (the azimuthal angle is set to be 0). Solving Eqs. (4) and (5) with a numerical method, the electron's motion in the laser field can be obtained. Then the radiation emitted from the interactions of a focused laser pulse with an electron can be calculated from Eqs. (6) and (7). Further, the angular spectral intensity (spectral intensity per solid angle) can be calculated by the Fourier transform of $\mathbf{A}(t)$ [33],

$$\frac{d^2I}{d\omega\, d\Omega} = 2|\mathbf{A}(\omega)|^2, \tag{8}$$

$$\mathbf{A}(\omega) = \frac{1}{\sqrt{2\pi}}\int_{-\infty}^{\infty}\mathbf{A}(t)e^{-i\omega t}\,dt. \tag{9}$$

The schematic geometry of Thomson scattering is shown in Fig. 1. In this figure, the laser is assumed to propagate in the $+\hat{\mathbf{z}}$ direction while the electron moves in the $-\hat{\mathbf{z}}$ direction with an initial energy γ_0. The electron is set at $(0,0,z_0)$ initially where $z_0=10L$. It has been shown that the radiation is collimated about the backscattered direction [22–24], and therefore we set $\theta=\pi$ in this paper. Further, we set the azimuthal angle $\varphi=0$ by the symmetry of the circularly polarized laser beam.

III. RESULTS AND DISCUSSIONS

First, we consider the temporal characteristics of the Thomson backscattering by an energetic electron. The time history of the radiated power per solid angle in the backward direction is shown in Fig. 2(a). Here the laser amplitude a_0 is 3, the beam waist b_0 is 30λ where the wavelength λ is 800 nm, L is 20λ (the corresponding pulse duration is about 100 fs), the initial electron energy γ_0 is 20, i.e., 10 MeV. Figure 2(a) shows that the emitted power has a twin-peak structure in time evolution. The emitted power rises rapidly at the beginning. Then it falls back quickly and keeps a much lower value, about 1% of its maximum, for 300 as. After that it rises again to its maximum and then falls back again. Thus, a 469 as crescent-shaped pulse with a peak power of about 150 W/rad^2 is generated. This crescent-shaped pulse can be interpreted from Fig. 2(b) which shows the corresponding z component velocity of the electron. At the beginning of the interaction, the electron acceleration increases quickly with increase of the driving laser intensity. Thus the radiated power increases quickly at the beginning. Meanwhile, the longitudinal ponderomotive force pushes the electron forward in the ascending front of the laser pulse. Therefore, the absolute value of the z component of electron velocity decreases at the beginning as shown in Fig. 2(b). As the driving laser intensity increases, the electron is decelerated efficiently; then the radiated power begins to fall back. While the ascending part of the laser pulse overtakes the electron, the longitudinal ponderomotive force pushes the electron backward in the descending part of the laser pulse. The absolute value of velocity increases in the descending part of

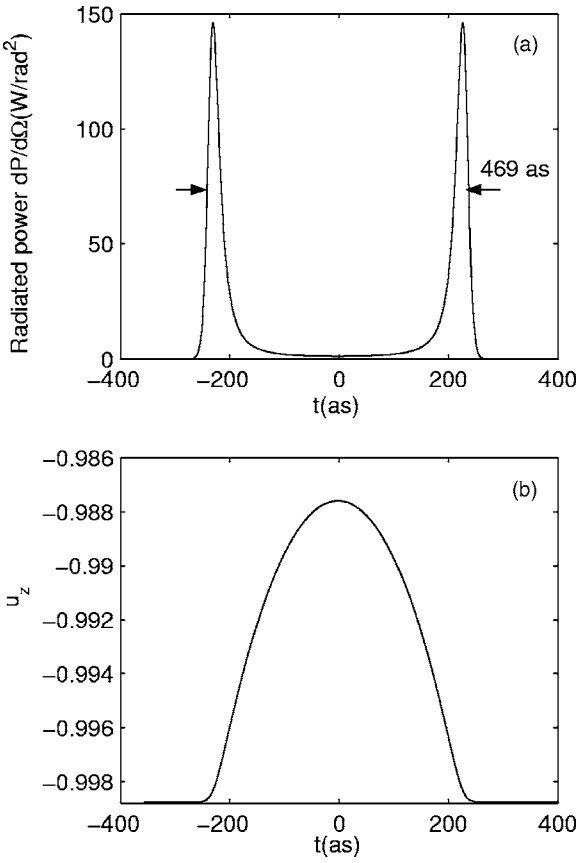

FIG. 2. (a) The time history of the radiated power per solid angle in a non-tightly-focused laser beam. (b) The corresponding z component of velocity of the electron. The parameters are $a_0=3$, $b_0=30\lambda$, $L=20\lambda$, $\gamma_0=20$. The time at which the laser pulse reaches its maximum is set as $t=0$ in this paper.

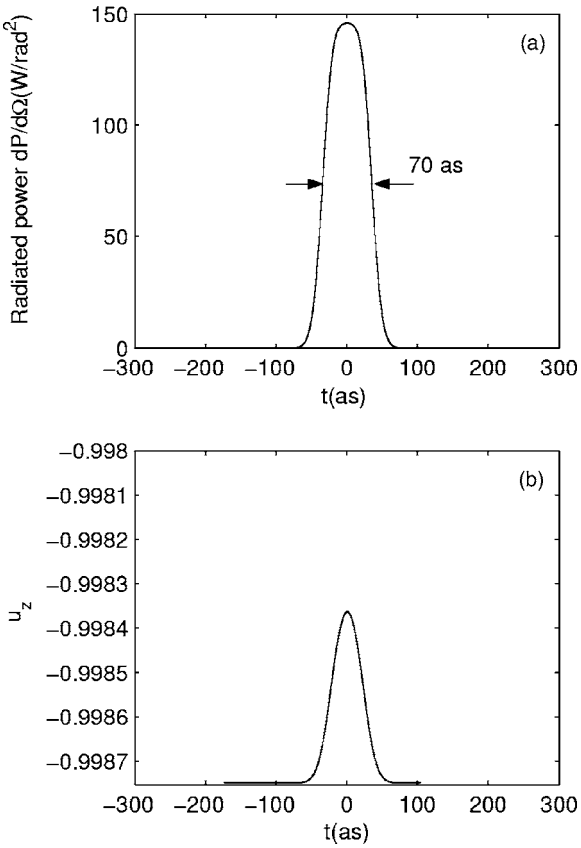

FIG. 3. (a) The time history of the radiated power per solid angle in a tightly focused laser beam. (b) The corresponding z component of velocity of the electron. The beam waist $b_0=3\lambda$ and the other parameters are the same as those in Fig. 2.

the laser pulse as shown in Fig. 2(b). Consequently, the radiated power increases with increase of electron velocity. Finally, as the laser intensity decreases, the radiated power decreases as well. Therefore a crescent-shaped pulse is obtained during the whole process.

The time history of the radiated power per solid angle in a tightly focused laser with a beam waist of 3λ is shown in Fig. 3(a). The other parameters are the same as those in Fig. 2. We see from Fig. 3(a) that the radiated power increases in the ascending part and decreases in the descending part of the driving laser pulse. During the whole process, a 70 as isolated pulse with a peak power of about 150 $\mathrm{W/rad^2}$ is generated. The corresponding z component velocity of electron is shown in Fig. 3(b). As shown in this figure, the absolute value of velocity decreases in the ascending part and increases in the descending part of driving laser pulse. But the velocity changes only 0.04% of its initial velocity. For the tightly focused laser beam, the laser intensity is higher at the focus where the ponderomotive force is stronger, and it becomes much lower at other regions where the ponderomotive force is weaker. As a result, the effective interaction length is shorter, the electron is decelerated inefficiently. So the variety of electron velocity is inappreciable. The radiated power is primarily determined by the acceleration of an electron or the driving laser intensity in the tightly focused laser case. As the laser intensity increases, the radiated power increases in the ascending part of driving laser pulse, while in the descending part of the driving laser pulse, the radiated power decreases with the decrease of the driving laser intensity. Finally, a single-peak pulse is generated in the whole process.

Figure 4 illustrates the dependence of the radiated pulse duration on the driving laser pulse duration. The solid line corresponds to the case of a non-tightly-focused laser with a beam waist of 30λ. The other parameters are the same as those in Fig. 2. As shown in Fig. 4, the duration of the radiated pulse increases linearly with increasing the driving laser pulse duration. This can be interpreted as follows. Because the absolute value of the z component of the electron velocity is greater than that for the x and y components, the interaction time of the electron with the laser field is limited to $2L/(1-u_z)$ approximately [24]. This indicates that as the driving laser pulse duration increases, the interaction time increases linearly, and the duration of the radiated pulse increases linearly as well. The dashed line shown in Fig. 4 corresponds to the case of a tightly focused laser with a beam waist of 3λ. As shown in this figure, the duration of the radiated pulse in a tightly focused laser beam increases slightly with increasing driving laser pulse duration. Compared to the result for a non-tightly-focused laser, the radiated pulse duration is much shorter in the

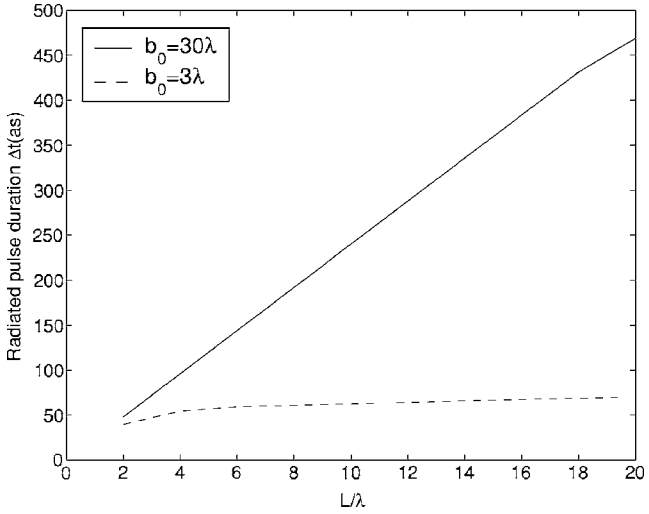

FIG. 4. The dependence of the radiated pulse duration on the driving laser pulse duration. The solid line corresponds to the case of a non-tightly-focused laser with $b_0=30\lambda$. The dashed line corresponds to the case of a tightly focused laser with $b_0=3\lambda$. The other parameters are the same as those in Fig. 2.

tightly focused laser case. This is because the effective interaction length and interaction time is shorter in a tightly focused laser.

The dependence of the radiated pulse duration on the electron initial energy in the cases of a non-tightly-focused ($b_0=30\lambda$) and a tightly focused laser beam ($b_0=3\lambda$) is shown in Fig. 5, respectively. The other parameters are the same as those in Fig. 2. It is shown in Fig. 5 that the duration of the radiated pulse decreases with increasing initial electron energy. It is consistent with the previous analysis about the duration of the emitted pulse. Furthermore, an interesting feature shown in this figure is that a zeptosecond pulse is generated in the scattering of an electron with an

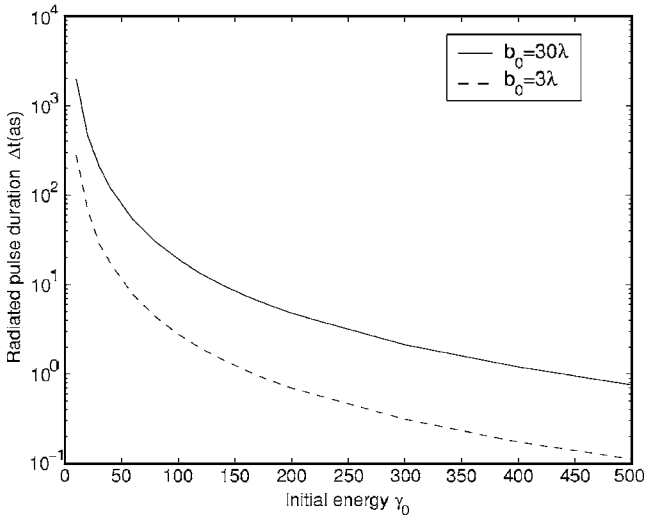

FIG. 5. The dependence of the radiated pulse duration on the initial electron energy in a non-tightly-focused (solid line) and tightly-focused (dashed line) laser beam. The parameters are the same as those in Fig. 2.

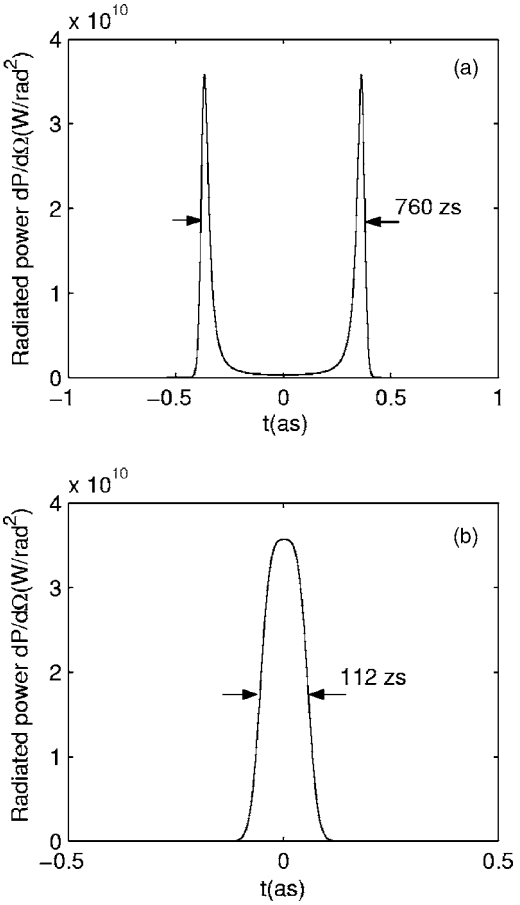

FIG. 6. The time history of the radiated power per solid angle in the case of (a) a non-tightly-focused and (b) a tightly focused laser beam, respectively. The initial electron energy $\gamma_0=500$ and other parameters are the same as those in Fig. 2.

initial energy of $\gamma_0=500$, i.e., 250 MeV. This can be clearly seen from Fig. 6 which shows the time history of the radiation in the case of a non-tightly-focused and a tightly focused laser beam, respectively. The initial electron energy $\gamma_0=500$ and the other parameters are the same as those in Fig. 2. As shown in Fig. 6(a), a crescent-shaped pulse with a duration of 760 zs is generated in the non-tightly-focused laser beam. While in the tightly focused laser case, a single-peak pulse with a duration of 112 zs is generated as shown in Fig. 6(b). Moreover, the radiated power increases up to 10^{10} W/rad^2 which is eight orders of magnitude higher than that in the scattering of an electron with an initial energy of 10 MeV.

Now, we discuss the spectral characteristics of the emitted ultrashort pulses. The angular spectral intensity of the attosecond pulse radiated in a non-tightly-focused laser beam is plotted in Fig. 7(a). As shown in this figure, the angular spectral intensity is low when $\omega<150\omega_0$. Then it increases quickly and is high until $\omega/\omega_0=1.63\times10^3$, at which it decreases to one-tenth of its maximum. In this spectrum, the harmonics modulation disappears in the scattering of a laser pulse which is consistent with the previous result [25]. As we know, the electron oscillates in the x and y directions and drifts along the z direction in a circularly polarized laser

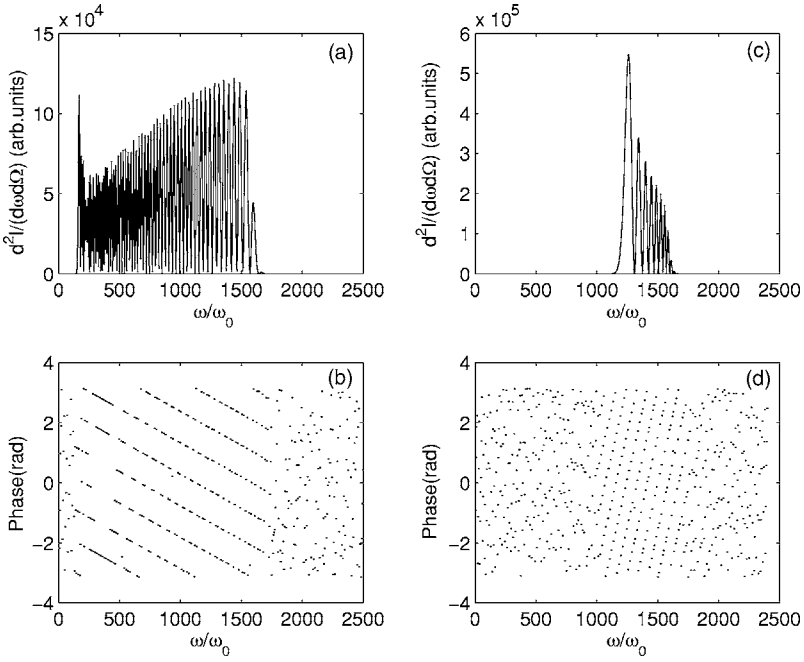

FIG. 7. (a) The angular spectral intensity and (b) phases of the corresponding frequency components of the radiated pulse shown in Fig. 2(a). (c) The angular spectral intensity and (d) phases of the corresponding frequency components of the pulse shown in Fig. 3(a).

field. Approximately, the average electron velocity is assumed as u_z. In other words, the average electron rest frame in which the electron is on the average at rest [21] moves with u_z with respect to the laboratory frame. The radiation frequency shifts due to the Doppler effect [21,26], and can be estimated as

$$\omega/\omega_0 = (1 - u_z)/(1 - u_z \cos\theta). \tag{10}$$

As shown in Fig. 2(b), $u_{zmin} = -0.998\,75$ and $u_{zmax} = -0.987\,59$. In our case, we consider the backscattering, i.e., $\theta = \pi$. The estimated frequencies are calculated as $(\omega/\omega_0)_{max} = 1.6 \times 10^3$ and $(\omega/\omega_0)_{min} = 160$ which are very close to our numerical values. The angular spectral intensity of the pulse radiated in a tightly focused laser beam is plotted in Fig. 7(c). As shown in this figure, the spectral intensity is higher in the range from $1.2 \times 10^3 \omega_0$ to $1.6 \times 10^3 \omega_0$, and is much lower at other regions. Compared to the spectrum for the crescent-shaped pulse, the monochromaticity of the single-peak pulse radiated in a tightly focused laser beam is much better. As shown in Fig. 3(b), the maximum of electron velocity is $-0.998\,36$, then the minimum frequency is estimated to be $1.22 \times 10^3 \omega_0$ according to Eq. (10). The maximum frequency is estimated to be $1.6 \times 10^3 \omega_0$. These estimates are consistent with our numerical results, which indicates that the monochromaticity and pulse shape of the

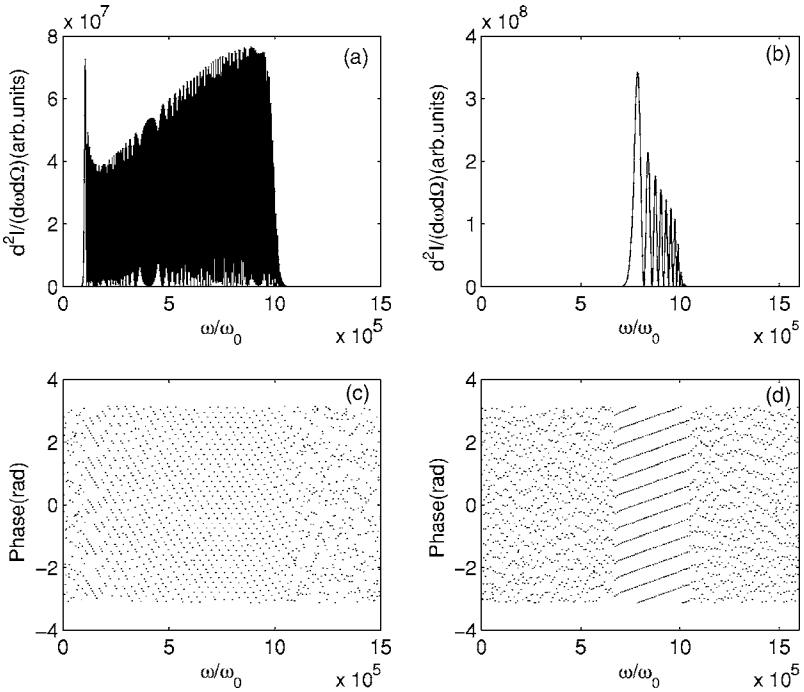

FIG. 8. (a) The angular spectral intensity and (b) phases of the corresponding frequency components of the radiated pulse shown in Fig. 6(a). (c) The angular spectral intensity and (d) phases of the corresponding frequency components of the pulse shown in Fig. 6(b).

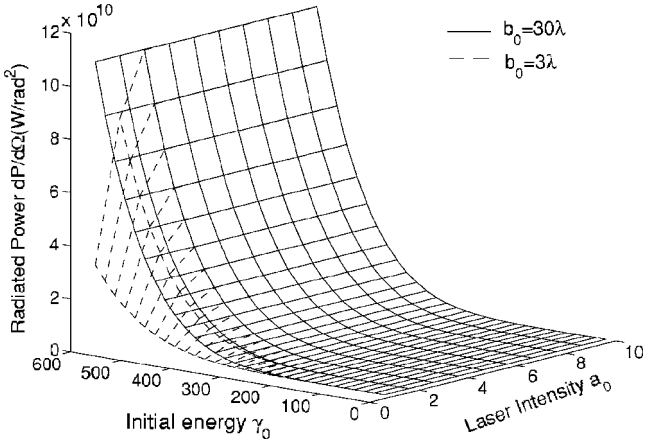

FIG. 9. The dependence of the peak power of the radiated pulse on the initial electron energy and the driving laser amplitude in the cases of a non-tightly-focused (solid line) and a tightly focused (dashed line) laser field, respectively. The other parameters are the same as those in Fig. 2.

emitted pulse can be modified by decreasing the driving laser beam waist. A near monochromatic attosecond pulse can be obtained in a very tightly focused laser field. This characteristic provides us another avenue to obtain a near monochromatic x-ray attosecond pulse. It is beneficial for some applications, such as γ-γ collisions, which require the generation of a single narrow x-ray or γ-ray pulse [25].

The phases of the frequency components in the spectrum shown in Fig. 7(a) are plotted in Fig. 7(b). As shown in Fig. 7(b), the phase behavior of the frequency components less than $150\omega_0$ is random. Following that, the phase behavior of the frequency components ranging from $150\omega_0$ to $1750\omega_0$ is more regular, even though they are not phase locked [7]. Then the phase behavior of the frequency components higher than $1750\omega_0$ gradually becomes out of order again. Figure 7(d) shows the phases of the frequency components in the spectrum shown in Fig. 7(c). It is clearly shown in Fig. 7(d) that the phase behavior of the frequency components ranging from $1000\omega_0$ to $1700\omega_0$ is more regular than that of the other frequencies. From Fig. 7, one can see that the phase behavior of the frequency components with higher intensity is regular. This result implies that these frequency components travel with the same speed, which can result in an ultrashort pulse.

The angular spectral intensity of the zeptosecond pulses radiated in a non-tightly-focused and a tightly focused laser beam is plotted in Figs. 8(a) and 8(c), respectively. The corresponding phases of the radiated frequency components are shown in Figs. 8(b) and 8(d), respectively. In a non-tightly-focused laser beam, the angular spectral intensity of the frequencies from $9.6\times10^4\omega_0$ to $1\times10^6\omega_0$ is higher and the phase behavior of these frequency components is more regular as shown in Figs. 8(a) and 8(c). However, in a tightly focused laser beam, the radiation is mainly in the range from $7.4\times10^5\omega_0$ and $9.9\times10^5\omega_0$ and the monochromaticity is much better as shown in Fig. 8(b). Moreover, it is clearly shown in Fig. 8(d) that the phase behavior of the frequency components ranging from $7\times10^5\omega_0$ to $1\times10^6\omega_0$ is more regular than the other frequencies. These results can be understood just as in the previous discussion.

Figure 9 shows the dependence of the radiated power on the electron initial energy and the driving laser amplitude. The solid and dashed lines correspond to the non-tightly-focused and tightly focused laser cases, respectively. As shown in this figure, the radiated power clearly increases with increasing initial electron energy. When the initial energy increases to $\gamma_0=600$, i.e., 300 MeV, the radiated power of the zeptosecond pulse increases up to 10^{11} W/rad^2. It is five orders of magnitude higher than that in the scattering by a group of electrons with a density of 10^{16} cm^{-3} [29]. Considering that the radiation is well collimated in a cone with a half angle of $\sim1/\gamma$ in the backward direction [22–24], the radiation is emitted in a narrower cone with increase of electron energy. Thus the actual total power may increase less rapidly. Furthermore, when $a_0<2$ the radiated power in a tightly focused laser is a little lower than that in a non-tightly-focused laser beam, while $a_0>2$ the radiated power is about equal in these two cases. As shown in this figure, the radiated power increases slowly with increasing the driving laser intensity. In a higher-intensity field, the electron acceleration is larger and then the radiated power is enhanced. On the other hand, the electron is decelerated more significantly in the ascending part of the laser pulse, the radiated power is reduced by this effect. On the whole, the radiated power in a higher-intensity field is not enhanced very much. Further numerical results show that the radiated power changes slightly with the variety of the driving laser pulse duration. From Figs. 6 and 9, one can see that the peak power and pulse duration of the emitted pulse at $\gamma_0=20$ are about 150 W/rad^2 and 70 as in the tightly focused laser case, the total energy of the emitted pulse is estimated to be about 10^{-5} nJ. The driving laser energy in the tightly focused laser case is about $0.2J$, and the efficiency of the radiation is about 10^{-13}. The efficiency can be improved by increasing the electron initial energy, e.g., it increases to about 10^{-8} at $\gamma_0=1000$. Another possible way to improve the efficiency is using the electron beam. However, this method has its drawbacks, such as the energy spread of the electron beam which may broaden the pulse duration of the radiation. The calculation indicates that the duration of the emitted pulse is still in the attosecond region as long as the energy spread is restricted within 4 MeV at $\gamma_0=20$ (10 MeV). Further more detailed investigations are still required. These results will be beneficial for both the understanding of the nonlinear Thomson scattering, and the future investigation and design of attosecond and zeptosecond x-ray sources.

IV. CONCLUSIONS

Nonlinear Thomson backscattering of an intense circularly polarized laser by a counterpropagating energetic electron is investigated. It is indicated that Thomson backscattering has the potential to produce attosecond and zeptosecond pulses. A crescent-shaped 469 as pulse can be generated in the scattering of a non-tightly-focused laser pulse with an intensity around 10^{19} W/cm^2 by an electron with the initial energy of 10 MeV. The radiation spectrum

is mainly in the range from 230 eV to 2.5 keV. With increase of the initial electron energy, the peak power of the radiated pulse increases and the pulse duration decreases. An isolated zeptosecond pulse can be obtained by an energetic electron with an initial energy above 200 MeV. The radiated pulse shape and monochromaticity can be modified by changing the laser beam waist. A single-peak attosecond pulse with a shorter pulse duration and better monochromaticity can be obtained in a tightly focused laser field.

ACKNOWLEDGMENT

The authors would like to thank Professor Dongsheng Guo for stimulating discussions and reviewing the manuscript. This work was supported by the National Natural Science Foundation of China under Grant No. 10375083, the National Key Basic Research Special Foundation under Grant No. TG1999075206-2, and the MOE Foundation for the Doctoral Program of China under Grant No. 20040487023.

[1] Nenad Milosevic, Paul B. Corkum, and T. Brabec, Phys. Rev. Lett. **92**, 013002 (2004).
[2] R. Klenberger *et al.*, Nature (London) **427**, 817 (2004).
[3] T. Brabec and F. Krausz, Rev. Mod. Phys. **72**, 545 (2000).
[4] Cy. Farkas and Cs.Tóth, Phys. Lett. A **168**, 447 (1992).
[5] S. E. Harris, J. J. Macklin, and T. W. Hansch, Opt. Commun. **100**, 487 (1993).
[6] Philippe Antoine *et al.*, Phys. Rev. A **56**, 4960 (1997).
[7] Philippe Antoine, Anne L'Huillier, and Maciej Lewenstein, Phys. Rev. Lett. **77**, 1234 (1996).
[8] I. P. Christov, M. M. Murnane, and H. C. Kapteyn, Phys. Rev. A **57**, R2285 (1998).
[9] T. W. Hänsch, Opt. Commun. **80**, 71 (1990).
[10] A. E. Kaplan, Phys. Rev. Lett. **73**, 1243 (1994).
[11] S. E. Harris and A. V. Sokolov, Phys. Rev. Lett. **81**, 2894 (1998).
[12] A. V. Sokolov, D. D. Yavus, and S. E. Harris, Opt. Lett. **24**, 557 (1999).
[13] K. Lee *et al.*, Phys. Rev. E **67**, 026502 (2003).
[14] P. M. Paul *et al.*, Science **292**, 1689 (2001).
[15] M. Hentschel *et al.*, Nature (London) **414**, 509 (2001).
[16] P. B. Corkum *et al.*, Opt. Lett. **19**, 1870 (1994); M. Y. Ivanov *et al.*, Phys. Rev. Lett. **74**, 2933 (1995).
[17] Fam Le Kien, Katsumi Midorikawa, and Akira Suda, Phys. Rev. A **58**, 3311 (1998).
[18] I. P. Christov, M. M. Murnane, and H. C. Kapteyn, Phys. Rev. Lett. **78**, 1251 (1997).
[19] N. M. Naumova *et al.*, Opt. Lett. **29**, 774 (2004).
[20] A. E. Kaplan and P. L. Shkolnikov, Phys. Rev. Lett. **88**, 074801 (2002); G. Stupakov and M. Zolotorev, *ibid.* **89**, 199501 (2002); A. E. Kaplan and P. L. Shkolnikov, *ibid.* **89**, 199502 (2002); W. R. Garrett, *ibid.* **89**, 279501 (2002); A. E. Kaplan and P. L. Shkolnikov, *ibid.* **89**, 279501 (2002).
[21] E. S. Sakachik and G. T. Schappert, Phys. Rev. D **1**, 2738 (1970).
[22] P. Sprangle, A. Ting, E. Esarey, and A. Fisher, J. Appl. Phys. **72**, 5032 (1992).
[23] E. Esarey, S. K. Ride, and P. Sprangle, Phys. Rev. E **48**, 3003 (1993).
[24] S. K. Ride, E. Esarey, and M. Baine, Phys. Rev. E **52**, 5425 (1995).
[25] F. V. Hartemann, Phys. Plasmas **5**, 2037 (1998).
[26] W. Yu, M. Y. Yu, J. X. Ma, and Z. Xu, Phys. Plasmas **5**, 406 (1998).
[27] S. Y. Chen, A. Maksimchuk, and D. Umstadter, Nature (London) **396**, 653 (1998); S. Y. Chen *et al.*, Phys. Rev. Lett. **84**, 5528 (2000).
[28] W. P. Leemans *et al.*, Phys. Rev. Lett. **77**, 4182 (1996).
[29] K. Lee, B. H. Kim, and D. Kim, Phys. Plasmas **12**, 043107 (2005).
[30] A. Yariv, *Quantum Electron*, 2nd ed. (Wiley, New York, 1975).
[31] Yousef I. Salamin, Guido R. Mocken, and Christoph H. Keitel, Phys. Rev. ST Accel. Beams **5**, 101301 (2002); J. X. Wang *et al.*, Phys. Rev. E **60**, 7473 (1999); Feng He *et al.*, *ibid.* **68**, 046407 (2003).
[32] P. Gibbon, IEEE J. Quantum Electron. **33**, 1915 (1997); Wei Yu *et al.*, Phys. Rev. E **66**, 036406 (2002).
[33] J. D. Jackson, *Classical Electrodynamics*, 2nd ed. (Wiley, New York, 1975).